Germinario *et al. Herit Sci* (2020) 8:87
https://doi.org/10.1186/s40494-020-00433-9

Heritage Science

RESEARCH ARTICLE Open Access

Taya Caves, a Buddhist marvel hidden in underground Japan: stone properties, deterioration, and environmental setting

Luigi Germinario[1*], Chiaki T. Oguchi[1], Yasuhiko Tamura[2], Sohyun Ahn[1] and Momoko Ogawa[1]

Abstract

The Buddhist sacred site of Taya Caves is a gem hidden underground in Yokohama, Japan. The caves were excavated and sculpted into bare rock by Shingon Buddhist monks from the Kamakura until the Edo period (thirteenth–nineteenth century), and dedicated to ascetic training, rituals, and pilgrimage. They are a maze of halls and galleries decorated with hundreds of rock-cut reliefs, picturing deities and masters of Buddhism, temples and shrines, real and fantastic animals, vegetal motifs, mandalas, zodiac signs, family crests, etc. The history and rock art of Taya Caves and the urge to preserve their cultural value led to this first-ever scientific investigation, dealing with the stone properties, deterioration, and environmental setting. Textural, mineralogical, geochemical, and petrophysical investigations were combined with a microclimate monitoring and chemical analyses of groundwater and rainwater. The caves are excavated into a clay-rich fossiliferous siltstone, extremely soft and porous and highly susceptible to water-driven weathering. Water represents a constant in Taya Caves, either flowing, dripping, and stagnant; or rising from the subsoil; or related to the extremely high relative humidity. Crusts and efflorescences represent important indicators of mineral dissolution and mobilization. The crusts are made of gypsum, crystallized from the dissolution of calcareous bioclasts and oxidation of pyrite, with minor calcite. The efflorescences are composed of chlorides, phosphates, sulfates, and carbonates, possibly deriving from agrochemicals and the surface vegetation cover. The salt weathering is strictly related to the microenvironmental variables and physico-chemical properties of the phases and waters involved. Rock-water interaction is particularly damaging even considering just the physical mechanisms. The stone is strongly sensitive to water absorption, hygroscopic adsorption, and slaking: the stresses generated by in-pore water and air movement and the swelling clay minerals may lead to rapid disintegration, especially during cyclic processes. This research is expected to raise concerns about the safeguard of Taya Caves and support future monitoring and conservation plans, and to foster a wider promotion and valorization of this heritage site.

Keywords: Rock art, Salt weathering, Gypsum crust, Efflorescence, Slaking, Microclimate monitoring, Groundwater chemistry, Siltstone decay, Pyrite, Swelling clay minerals

Introduction

Caves in heritage science

The research on properties, weathering, and conservation of natural stone in cultural heritage is largely devoted to open-air monuments, historical architecture, and archaeological standing structures, whereas underground sites usually receive scarcer attention. This disparity recurs in heritage protection at institutional level. Among the 908 sites of cultural or mixed value inscribed in the UNESCO's list of World Heritage Sites, less than sixty (about 6%) include caves, hypogea, mines, rock-hewn architecture, and subterranean settlements.

Yet the underground cultural landscape has a relationship with human activities persisted for tens of thousands of years, involving religious and artistic practices,

*Correspondence: luigi.germinario@gmail.com
[1] Department of Civil and Environmental Engineering, Saitama University, 255 Shimo-Okubo, Sakura-ku, Saitama-shi, Saitama-ken 338-8570, Japan
Full list of author information is available at the end of the article

sheltering and housing, burial, food production and storage, exploitation of raw materials, etc. [1, 2]. From a scientific viewpoint, it represents a natural or semi-natural setting entailing a variety of environment-material interactions, which are much different from those in built heritage. The multidisciplinary approach is fundamental.

Cave vulnerability can be evaluated by different risk factors: geological-geomorphological (structural and slope stability, seismic events, etc.); environmental (water interaction and weathering); biological (biomass growth); and anthropic (human presence, site planning, local urbanization and exploitation of natural resources) [3]. The risk can be quantified and mapped with the support of geographic information systems and numerical modelling [4, 5]. Anthropic factors are often the most critical, and indirectly increase the environmental and biological risks. Visitors alter the cave microclimate, introduce new organic matter and microorganisms, and sometimes cause vandalistic damage [6, 7]; the increased air temperature and CO_2 level, associated with tourist flows, may accelerate condensation phenomena and cave wall corrosion [8–12].

Investigating those risk factors allows for a deeper comprehension of deterioration processes, which may be extremely severe and affect both the cave structure and rock art, namely sculpted and painted surfaces. Weathering patterns are widely discussed in the literature about monument decay [13–15] and their characteristics are analogue in the cave environment, although their origin and time evolution are dissimilar. Generally, closer attention needs to be reserved to water-related decay, e.g., salt weathering, mineral dissolution, and biodeterioration.

What requires a different perspective is cave conservation. First, the planning, documentation, and future evaluation of any conservation campaign greatly benefits from a continuous environmental monitoring, of air (temperature, humidity, CO_2 and Rn levels, airflows), water (composition, physical parameters, hydrogeology), and illumination; and graphic representation, often based on 3D digital reconstruction techniques nowadays [16, 17].

Conservation and restoration treatments may target the cave and rock art directly. Some examples include surface cleaning, consolidation, structural reinforcement, biocide application, removal of debris, dust, mud nests, and trash. Indirect measures involve the management of the site and its surroundings: adjustment of visitor density and lighting regime, control of moisture and water flow, installation of microclimate buffer zones, maintenance of protection barriers and trails, restriction of the local residential, commercial, and infrastructural development, farming, deforestation, etc. Overall, the golden rule is to maintain the microenvironmental conditions as stable as possible. If the site or visitors are in danger, closing the show cave, temporarily or permanently, represents an arduous but recommended decision [7, 16–19].

Aim

This study addresses Taya Caves (田谷の洞窟), a Buddhist sacred site in Yokohama, Kanagawa prefecture, central Japan. The history and rock art enshrined in Taya Caves, their allure, and the urge to comprehend, preserve, and promote their cultural value led to this first-ever scientific investigation, dealing with stone properties and deterioration, set against the environmental background. The cave vulnerability was evaluated through an experimental approach involving the analysis of microenvironmental variables, i.e., air temperature, relative humidity (RH), and water chemistry; and textural, mineralogical, geochemical, and petrophysical properties of the rock of the caves. Close attention is paid to the environmental constraints of stone deterioration, with emphasis on salt weathering and rock-water interaction. Elements of interest lie in the studied lithology, relatively unusual in caves, and the surprising conservation of the rock art, despite the extreme material weakness.

Being the first research on this theme, the results are expected to support future conservation plans. The complementary goal is to foster a wider promotion and valorization of the site, little known presently.

Historical background

The Buddhist practice of retiring to isolated underground places for worship and meditation originated in India, where, from as early as the third century BCE, monks had excavated grottoes into the side of cliffs, adorning them with altars, sculptures, carvings, and murals. The artistic outcomes were sometimes outstanding, like in the Deccan cave temples of Maharashtra. Compared to open-air timber architectures, cave temples offered better durability and protection against weather adversities, natural catastrophes, and human-made disasters. There, monks could pursue ascetic rituals in isolation and quietness while benefitting from a settled life [20, 21].

This practice spread in East Asia as Buddhism gradually made new proselytes, reaching Japan in the sixth century CE through the Korean Peninsula. Many caves frequented by monastic communities and examples of religious rock art are located in the Kanto region, in central Japan: Iwaya in Enoshima, Benten Kutsu in Kamakura, Oya-ji in Utsunomiya, Nippara in Okutama, Tamagawa Daishi in Tokyo, etc.; not to mention the countless mountain grottoes dedicated to prayer and burials.

Taya Caves are a gem off the beaten track, hidden in the outskirts of Yokohama, excavated into a hillside in the grounds of Josen-ji temple. Their history seems to begin during the thirteenth century (Kamakura period), when the region became the new political and cultural center of Japan, after the first shogun's government was established in the nearby city of Kamakura. The early times of Taya Caves are allegedly associated with the figure of a fleeing samurai, Asahina Saburo Yoshihide, and later with the local religious community of Tsurugaoka Hachimanguji Nijugo-bo. This community was formed by Buddhist monks of the Shingon Esoteric sect, who excavated the caves and dedicated them to ascetic training and rituals: during their quest for enlightenment, the disciples used to practice meditation, fast for weeks, and work for enlarging the underground spaces while praying and chanting. The countless chisel marks still visible in the interior are the evidence of a long and strenuous manual work. Today, Taya Caves appear as a maze of halls and galleries extending for 570 m on three floors, with the walls and ceilings carved with about 300 rock-cut high and low reliefs, many displaying fine artistic quality. The sculptures picture deities and masters of Buddhism, temples and shrines, real and fantastic animals, vegetal motifs, mandalas, zodiac signs, family crests, etc. (Fig. 1, Fig. 2) (video). They were created in the mid-nineteenth century (late Edo period), when soon enough the caves became a destination of religious journeys. The believers who could not afford trips in far regions of Japan, would visit Taya Caves and worship the carved images symbolizing the Shikoku pilgrimage and the Kannon pilgrimages of Bando, Saigoku, and Chichibu: that was a way to complete long spiritual routes – among the most popular traditional pilgrimages in Japan – in only one day, by visiting one single sacred site [22]. Although Taya Caves are registered and formally safeguarded as Japanese Cultural Property, they are little known, even more so overseas, and far from the main tourist circuits, despite their allure and historical significance.

Experimental

The first part of this study focuses on the environmental setting of Taya Caves. Exploratory site surveys initially involved only the microclimate, later combined with further investigations.

A long-term microclimate monitoring was carried out for 19 months, from June 2018 to January 2020, recording air temperature and RH in six different locations inside the caves, and one outside (Additional file 1), using Hygrochron data loggers by KN Laboratories (accuracy of ± 0.8 °C and ± 5% RH, resolution of 0.5 °C and 0.6% RH, and sampling rate of one measurement per hour).

Water chemistry was determined on samples of: groundwater, collected in the caves in two locations from May 2019 to January 2020, once per month; rainwater, collected uninterruptedly during the summer of 2019 (June–September) and the winter of 2019–2020 (December–February); water of the pond near the cave entrance, collected three times from October 2019 to January 2020 (Additional file 1). The water samples were filtered at 0.45 μm and their major-ion chemical composition was analyzed by ion chromatography (IC), using a chromatograph Shimadzu Prominence HIC-NS, a non-suppressor system with a conductivity detector working in a measurement range of 0.01–51,200 μS/cm. The water pH was also assessed by a visual colorimetric method known as Pack Test, by Kyoritsu Chemical-Check Lab. Corp, mixing the samples with suitable reagents.

The second part of this study concerns the properties of the rock that Taya Caves are excavated into, its decay patterns, and the weathering products detected on the cave surfaces. The on-site surveys were followed by the laboratory investigation of samples collected all through the caves – 30 small solid and powder samples from the altered rock (Additional file 1), in addition to massive blocks of fresh rock.

A basic petrographic characterization was achieved by the examination of thin sections at the polarized-light microscope.

Further information on mineralogy, texture, and microchemical composition was obtained through analyses at the scanning electron microscope (SEM): 15 carbon-coated samples – thin sections, cross sections, and irregular solid and powder samples – were analyzed with a microscope Hitachi S-3400 N, equipped with a W cathode operated at 15 kV, detectors for secondary and back-scattered electrons (SE and BSE), and a system for energy-dispersive X-ray spectroscopy (EDS) Bruker Quantax 400 with a detector XFlash 4010.

Mineralogical composition was determined by X-ray diffraction (XRD), with a diffractometer Rigaku Ultima III equipped with a Cu anode operated at 40 kV and 40 mA, measuring in the range 3–75°2θ with scan steps of 0.02°2θ and scan speed of 1 to 4°2θ/min. The measurements were done on 27 samples ground to fine powders.

Bulk geochemistry, accounting for the major- and trace-element composition, was analyzed by X-ray fluorescence (XRF), using a spectrometer Panalytical Axios operating in wavelength-dispersive spectroscopy (WDS) mode. Elemental quantification was obtained applying the fundamental-parameter method. The analyses were performed on 16 samples prepared as pressed powder pellets. Loss on ignition (LOI) was also determined separately.

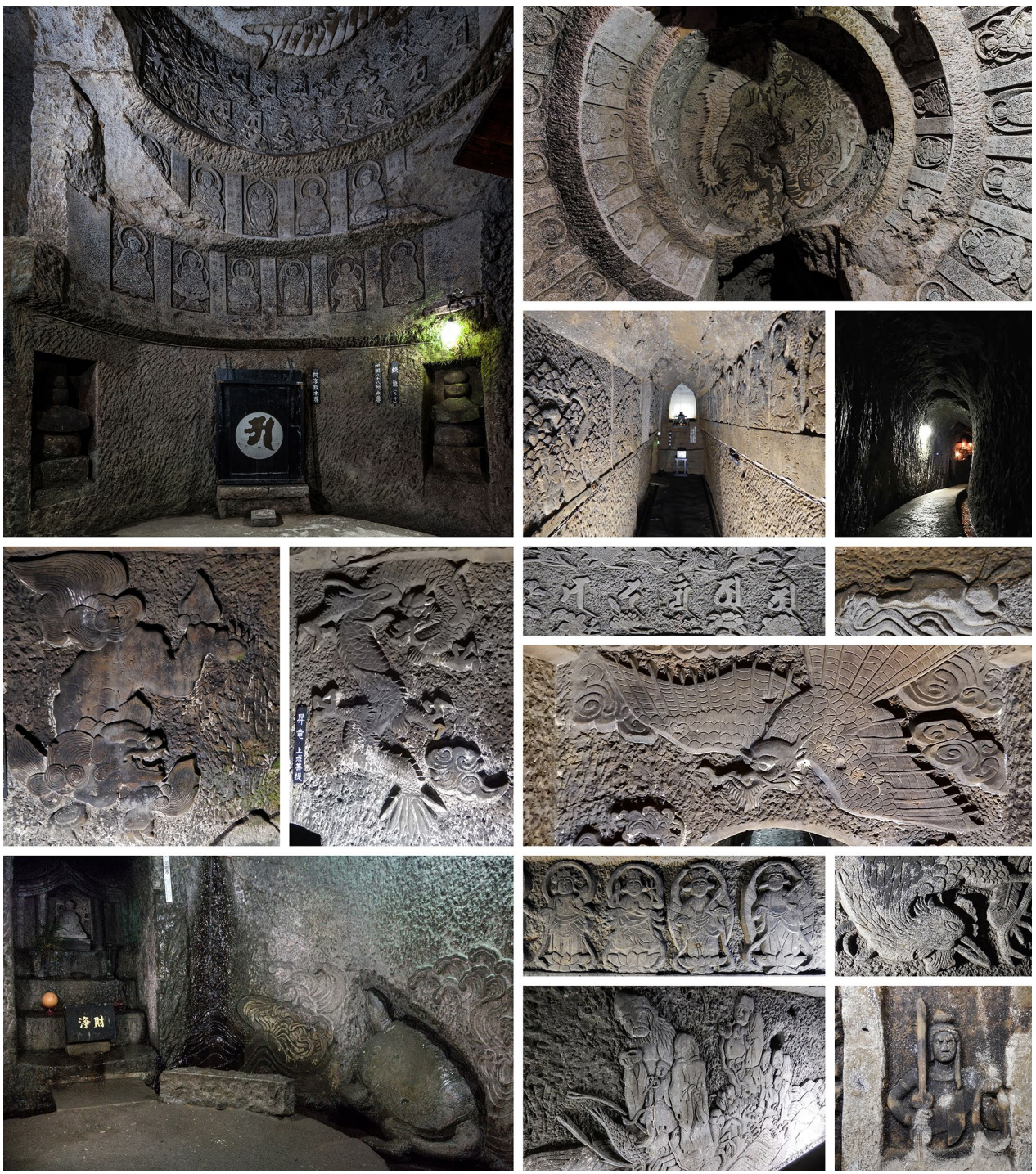

Fig. 1 Taya Caves: halls, galleries, and rock art

Porosity and pore-size distribution were measured by mercury intrusion porosimetry (MIP) according to the ASTM standard D4404 [23], with a porosimeter Micromeritics AutoPore IV 9500, covering a pore range of 0.005–800 μm, on 10 samples having a mass of 0.5–1 g. Complementary calculations of bulk and matrix density were also obtained.

Rock-water physical interaction was tested measuring the following properties: (a) Water absorption in total immersion at atmospheric pressure and water absorption

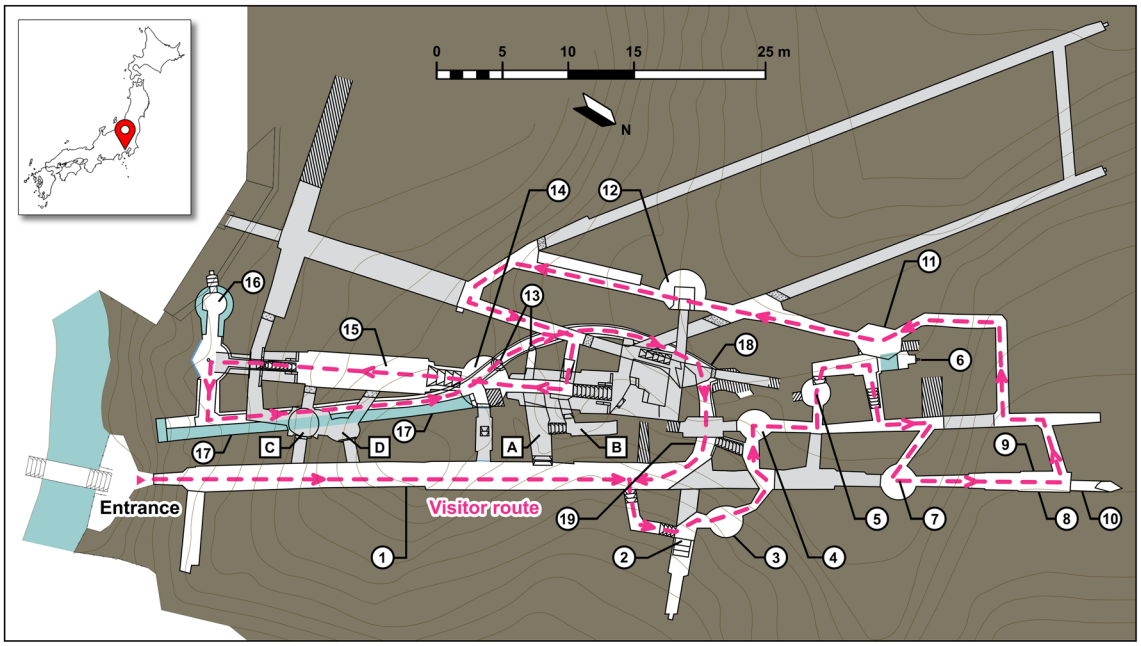

VISITOR ROUTE (~250 m)

1) A-Un lions • ascending-descending dragons • god Karura • family crests
2) Yakushi-dō temple
3) zodiac animal signs • bats
4) Chichibu 34 Kannon sacred sites • Karyōbinga
5) Chichibu 34 Kannon sacred sites • family crests
6) Asahina's god Benzaiten
7) Saigoku 33 Kannon sacred sites
8) Saigoku 33 Kannon sacred sites
9) Sone Tenman-gū shrine • pine trees of Takasago and Karasaki
10) master Kōbō-daishi warding off evil • Goryō shrine
11) Sanskrit seed-characters of the Taizōkai mandala • patterned family crests • crane
12) Shikoku 88 sacred sites • master Kōbō-daishi for one wish • rabbits
13) god Nitten • god Gatten
14) Shikoku 88 sacred sites • Sanskrit seed-characters of the Shijūku-in mandala • Gorintō pagodas • coiled dragon
15) Wisdom Kings Godai Myō-ō
16) turtle of Mt. Sada • master Kōbō-daishi of water • Ishidōmaru of Mt. Kōya • birds and dragonflies • bodhisattva Unchū Kuyō
17) disciples Rakan
18) Wisdom King Iwaya Fudō Myō-ō
19) Bandō 33 Kannon sacred sites

RESTRICTED AREAS

A) phoenix • peacock
B) bodhisattva Jizō • buddha Yakushi
C) disciples Rakan
D) Karakusa vegetal pattern

Fig. 2 Map of Taya Caves, with the list and location of the main rock-cut sculptures. The areas not accessible to visitors are in pale grey, the bodies of water in pale blue, and the surface covered by the hill above is in dark grey

rate, as per EN standard 13755 [24], on 4 bulk samples. (b) Hygroscopic water adsorption and desorption, as per EN ISO standard 12571 [25], on 8 bulk samples: they were oven-dried, placed in a climatic chamber at a constant temperature of 23 °C, and then subjected to a RH increase through the sequence 30–50–70–80–85–90–95–98%, and a subsequent decrease through the same steps. (c) Slake durability, assessed with the jar slake test following the indications by Santi [26], on 8 bulk samples: they were oven-dried, then immersed in water, and their slake category was recorded after 5–10-15–30 min and 1–2-4–24-48 h.

The analyses and testing were carried out at Saitama University, in the laboratories of the Comprehensive Analysis Center for Science and of the Department of Civil and Environmental Engineering.

Environmental setting

Microclimate monitoring

The climate of the Kanto region in central Japan is characterized by hot, humid summers, and cold, dry winters, with the rainy season occurring from early June to mid-July [27]. From the climatic data of Yokohama, August is the warmest month (averaging 27 °C, with mean maxima of 31 °C) and January the coldest (averaging 6 °C, with mean minima of 2 °C)—temperature very seldom drops below 0 °C. Summer months have an average RH of about 77%, which drops to 54% in wintertime. Precipitations are the highest in summer and early fall (especially in June, September, and October), amounting to 1700 mm yearly [28]. In that period, the number of rainy days almost reaches the number of days with no or minor precipitation (< 0.5 mm). Typhoons represent the most important

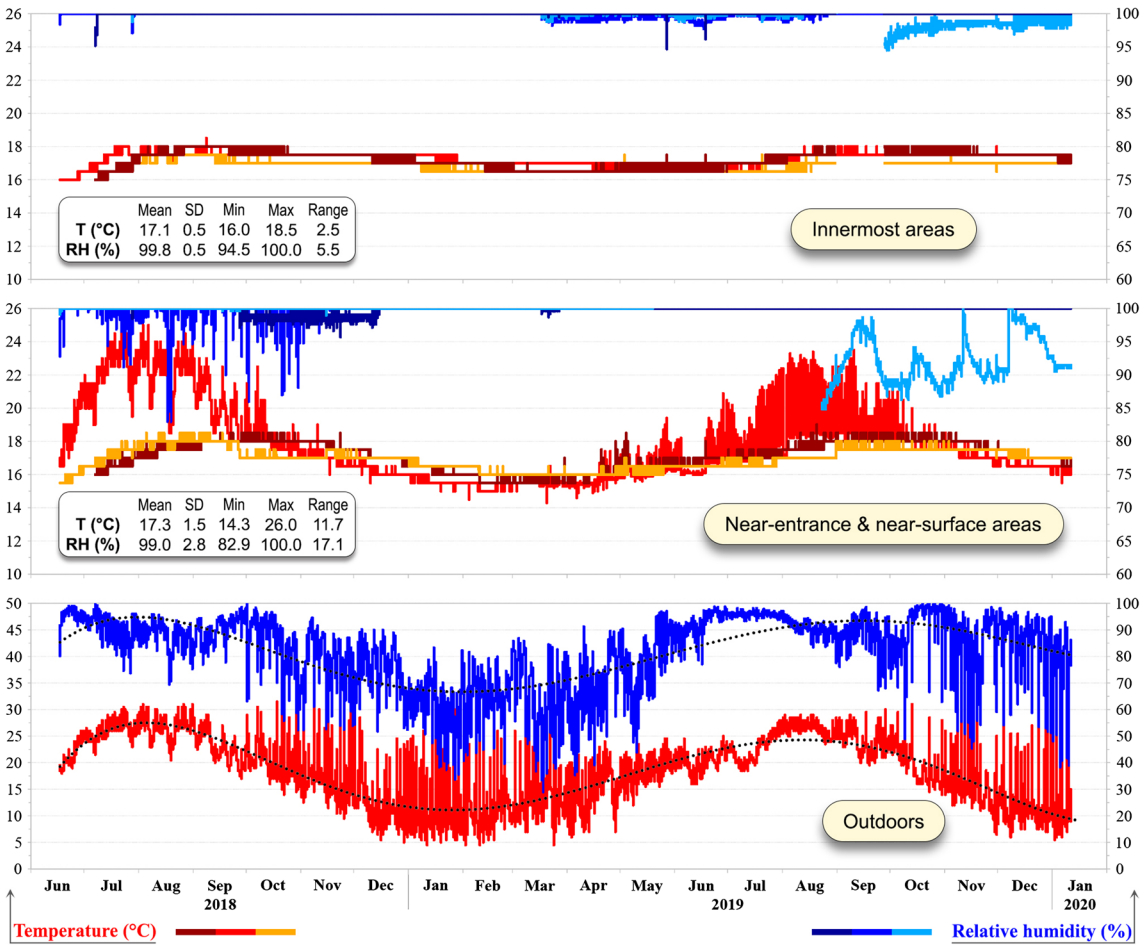

Fig. 3 Monitoring of air temperature and RH inside Taya Caves and outdoors. The interior measures are displayed in two groups, three monitoring sites each, based on their location (for each site, the temperature and RH trends have matching color brightness, as per the color scales at the bottom)

extreme weather events, and generally hit the region with violent winds and rainfalls in summer and early fall, most frequently in August and September [29].

In Fig. 3, the data of air temperature and RH collected inside Taya Caves are showed.[1] As reference, the measures recorded outside the entrance are also presented.[2] The microclimate of Taya Caves is characterized by a mean temperature of about 17 °C and an extremely high RH close to 100%, both essentially constant all year long. Nevertheless, temperature and RH vary more near the surface: the former replicating the outdoor seasonal fluctuations, the latter often dropping significantly from the saturation point, reflected by higher values of standard deviation and range. The three relevant locations, defined in Fig. 3 as near-entrance and near-surface areas, include the entrance gallery and the surroundings of the Turtle hall (Fig. 2; Additional file 1). Along the entrance gallery, the temperature difference between winter and summer may be over 10 °C, and RH can register large deviations from the typical near-100% values, decreasing to about 85%. These conditions represent an evidence of the influence of external airflows.

The microclimate setting of the near-entrance and near-surface areas deserves further considerations. First, all those locations are in the southern part of Taya Caves and on the southern flank of the hill, so they get a prolonged exposure to sun and, in summertime, also to the prevailing southerly winds [28]: these represent further reasons for the relevant dryer microclimate. Moreover,

[1] The RH data need to be taken with caution, their accuracy being affected by the technical limitations of the sensors, the extreme moisture, and condensation phenomena. For the same reason, some records are incomplete.

[2] These measures are conditioned by the particular microenvironmental conditions of the caves and the surrounding vegetation cover.

Table 1 Chemical composition by IC and pH of the groundwater in Taya Caves, the water of the nearby pond, and rainwater, averaged over the 2019 and 2020 samplings

	Caves' interior		Caves' exterior	
	Turtle hall	Asahina's Benzaiten	Pond	Rain
Na^+	11.0 (± 1.4)	6.9 (± 0.7)	9.6	1.3
Mg^{2+}	7.7 (± 1.4)	4.4 (± 0.9)	8.5	0.2
K^+	2.0 (± 0.4)	1.4 (± 0.2)	2.8	1.1
Ca^{2+}	32.9 (± 12.2)	12.8 (± 3.8)	31.6	0.7
	Caves' interior		Caves' exterior	
	Turtle hall	Asahina's Benzaiten	Pond	Rain
NO_3^-	0.4 (± 0.2)	0.4 (± 0.1)	0.6	0.1
SO_4^{2-}	26.5 (± 5.0)	19.8 (± 3.3)	47.9	2.6
Cl^-	22.6 (± 2.3)	8.6 (± 1.1)	20.0	2.4
	Caves' interior		Caves' exterior	
	Turtle hall	Asahina's Benzaiten	Pond	Rain
pH	7.5 (± 0.2)	7.2 (± 0.2)	7.4	6.3

Ion concentrations are in ppm, pH is dimensionless

The values in parentheses are standard deviations

it is worth noting that the Turtle hall is nearby old secondary entrances, which were permanently closed with their walls secured after major collapses occurred during the Great East Japan Earthquake of 2011; therefore, until about ten years ago, all the surroundings were less humid and in constant, direct connection with the external environment, just like the current entrance gallery. The last thing to report is the first-time installation in October 2018 of a stainless-steel door at the main entrance, open only during the visiting hours, every day from 9:30 a.m. until 4:30 p.m.; while this did not produce any significant microclimate change in the innermost caves, in the entrance gallery the standard deviations and ranges of temperature and RH registered after the door installation are appreciably lower than before.

The cave microclimate is probably not much affected by the usually low and inconstant visitor flow, which is mostly concentrated during weekends and the holidays in May and August.

Water chemistry

The microenvironment of Taya Caves is characterized by the constant presence of water, either flowing, dripping, and stagnant, or related to the extremely high RH. Water infiltrates and percolates through the vaults, rises from the subsoil, condensates, streams, and accumulates, wetting many stone surfaces.

The chemical properties of the water sampled inside and outside Taya Caves are summarized in Table 1. The groundwater shows analogue composition patterns in the two inner locations, with Ca^{2+} cations and SO_4^{2-} and Cl^- anions predominating: they record average concentrations of 23, 23, and 16 ppm, respectively, and maxima amounting to 51, 35, and 27 ppm. However, the groundwater from the Turtle hall, if compared to the samples collected near Asahina's Benzaiten (Fig. 2; Additional file 1), generally reports higher mineralization—i.e., the ion concentrations are almost two-fold on average—as well as higher chemical variability—in terms of standard deviations. The former spot, closer to the cave entrance, includes a body of flowing water fed by a stream seeping from the wall, whereas the latter, in a deep area, represents a body of mostly stagnant water: these observations might explain the compositional differences. Similar ion ratios were also detected in the water from the pond near the cave entrance. The bodies of water mentioned have a pH typically between 7.0 and 7.5, and the common composition of low-mineralization freshwaters [30–33]. These results can be compared to the chemistry of rainwater: its pH is slightly acid (6.3) and all the ion concentrations are much lower (e.g., about 1 ppm for Ca^{2+}, 3 ppm for SO_4^{2-}, and 2 ppm for Cl^-).

In light of these remarks, the composition of the groundwater of Taya Caves derives from the enrichment mainly in Ca^{2+}, SO_4^{2-}, and Cl^- of rainwater and surface

waters. During the infiltration into the soil of the hill and the percolation through the rock pores, water dissolves rock-forming minerals and other inorganic and organic compounds. The same applies to water capillary rise from the subsoil [32, 34].

One last comment is about the time variation of groundwater composition. The common trend shows the ion concentrations decreasing from summer to winter, this being probably connected with the higher precipitations in summertime, which entail enhanced rock-water interaction and leaching phenomena.

Petrological characteristics

Taya Caves are excavated into the outcrops of the Naganuma Formation of the Sagami Group, a sedimentary unit of the western Tokyo Bay dated to the Middle Pleistocene (0.5 Ma). The formation mostly includes marine siltstones and sandstones, with intercalated tuff layers, and in the lower part yields a number of neritic fossil species [35–37].

Taya stone is a very soft and porous siltstone, grain-supported and well sorted, composed mainly of quartz, plagioclase, and lithoclasts. The majority of the lithic fragments are very fine grained and constituted of clay minerals mostly of the groups of illite and smectite (montmorillonite-vermiculite composition). Other phases detected in minor amounts include actinolite, chlorite, zeolites (mordenite, stilbite, and laumontite), biotite, zircon, pyrite, and oxides of Fe and Ti. The grains are characterized, on average, by low sphericity and sub-angular to sub-rounded shape. The abundant intergranular porosity is filled sometimes with a clay-rich matrix.

A brown and a grey rock facies can be distinguished in Taya Caves. Besides the color, the main difference is the occurrence of a number of bioclasts and a relatively high concentration of pyrite in the grey facies, contrarily to the brown facies (Figs. 4, 5). The calcareous bioclasts include foraminifers, bivalves, gastropods, ostracods, echinoderms, and algae, can be very coarse and reach the size of several centimeters, although they are also finely dispersed in the rock matrix. Pyrite occurs in the matrix too, but many crystals fill the fossil intraparticle porosity, exhibiting a framboidal and multi-framboidal texture [38, 39]. Pyrite represents the diagenetic product of detrital Fe minerals reacting with the H_2S formed after the bacterial reduction of dissolved sulfates [40]; this activity is fostered by organic matter, which is particularly abundant in bioclastic sediments, explaining the pyrite replacement of mollusk soft parts, aragonitic shells and their organic matrix, and formation of internal molds of chambered shells [41, 42].

Overview of stone deterioration

The surveys conducted in Taya Caves disclosed the following stone deterioration patterns, classified according to the ICOMOS' indications [13].

Cracking phenomena are evident throughout the caves, on carved and non-carved elements, as small fractures or even extended splitting on vertical surfaces. Partial collapses of the sculpted ceiling in some halls are also noticeable. Other forms of detachment, more localized, include disintegration, scaling, and peeling—the last, principally along the entrance gallery. Features induced by material loss, in particular erosion, are more evident on the sculpted elements, with their original surface and details fading, the edges rounding, and parts missing. A specific type of differential erosion affects the grey rock facies, with the selective removal of fossil fragments, leaving surface cavities. One last point to report about the physical damage is the engraving of vandalistic graffiti.

As for the deterioration patterns involving surface alteration of chemical composition and color, the surveys revealed the occurrence of black crusts, pinkish efflorescences, black and orange patinas, and soiling from candle smoke. The crusts and efflorescences are localized in the galleries and halls of the lowest levels of the caves, on the first floor, relatively near the entrance. The crust growth may jeopardize the readability of the carvings.

Finally, it is worth mentioning the widespread biological colonization, involving a diffuse growth of whitish crustose lichens, the presence of phototrophic organisms, i.e., moss, algae, and other lower plants near electric light sources, and the penetration through the cave ceiling of roots of the higher plants growing on Taya hill. The root growth is visibly associated with rock fractures.

Some examples of the decay patterns mentioned are showed in Fig. 6.

Chemical alterations

Composition and microstructure

The black crusts are constituted by gypsum crystals ($CaSO_4 \cdot 2H_2O$) of diverse size and habit, tabular, prismatic, bladed, acicular, or lenticular in rosette-shaped aggregates. The crusts are often characterized by a composite stratigraphy, with an intermediate layer of finer-grained calcite ($CaCO_3$) in between the surface gypsum and the host rock (Fig. 7). Their dark color is due to carbonaceous matter entrapped in the crystalline gypsum mesh. The crusts can be over 1 mm thick, and are more compact than the substrate, i.e., with a porosity over 50% lower than that of the rock (see Porosity). A buffer zone between the stone surfaces with gypsum crusts and those without major chemical alteration is affected by a slight

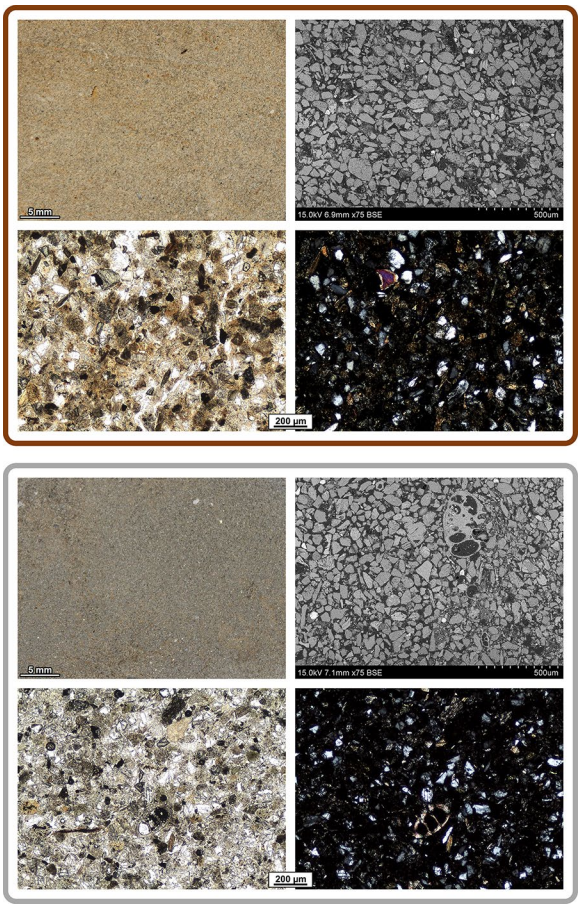

Fig. 4 Hand-specimen photographs (*top-left*) and thin-section photomicrographs at the SEM-BSE (*top-right*) and optical microscope in plane- and cross-polarized light (*bottom*), differentiating between the brown and the grey facies of Taya stone

early sulfation. The composition differences are better explained by the bulk chemical analyses (Table 2): the crusts report concentrations of SO_3 and CaO of about 39 and 33%, respectively—versus 1 and 4% from the substrate—whereas the early sulfation entails only a moderate deviation from the silicate rock composition. The trace-element composition indicates the scarce influence of external air pollution, which generally is responsible of high heavy-metal concentrations in black crusts [43–45].

As for the efflorescences, their composition was determined by the SEM microanalyses, revealing high concentrations of P, Cl, S, as well as K and Ca, and lastly Mg, all not strictly attributable to the mean silicate rock composition and detected on spots without visible preserved fossils (Fig. 8). This composition seems to be given overall by mixed chlorides, phosphates, sulfates, and carbonates. That is also corroborated by the bulk chemical analyses, e.g., revealing high enrichments in Cl—with a concentration up to 0.2%, that is, about ten-fold that in the rock—and P_2O_5—over three-fold (Table 2). A precise phase determination could not be achieved by XRD, probably because of the low crystallinity and the very fine grain size, except for the identification of gypsum, calcite, and apatite ($Ca_5(PO_4)_3(F/OH/Cl)$). The presence of K-chlorides is also likely.

Finally, minor chemical alterations, affecting the stone color, are produced by black or orange patinas, generally characterized by a high Fe content, and a slight enrichment in Mn. The main component of the orange patinas is goethite (FeO(OH)), and their Fe_2O_3 concentration is almost four-fold that of the bulk rock (Table 2).

Sources

Gypsum

The origin of gypsum in a non-carbonate rock like Taya stone, with relatively low Ca and S content, and with no significant contribution from extrinsic air pollutants or other geomaterials in the cave structure, is explained by the dissolution and interaction of two rock components: calcareous bioclasts and pyrite (FeS_2). The fabric-selective dissolution of calcareous bioclasts is a well-known process generating moldic porosity [46], and has been recognized in Taya Caves as differential erosion (see Overview of stone deterioration). The reaction of $CaCO_3$ dissolution releases Ca^{2+} and HCO_3^-, and has higher kinetics in acid solutions (especially when pH is below 6 or 5) whereas, in basic and alkaline solutions, rather precipitation is favored [47–52]. Pyrite is the most common species involved in mudrock weathering, and can alter when exposed to air at any pH value, with higher kinetics when in contact with water and in framboidal minerals [53–55]. Pyrite oxidizes to Fe-oxides and hydroxides (e.g., goethite, hematite) producing H_2SO_4. The final stage involves the reaction of the dissolution products, i.e., mobilized Ca^{2+} or recrystallized $CaCO_3$ from fossils and H_2SO_4 from pyrite, leading to gypsum crystallization, which can happen as shortly as in few weeks or months [56].

There are several experimental clues that allow for recognizing these processes as the principal driving forces of the formation of gypsum crusts in Taya Caves. First, a spatial correspondence: bioclasts and pyrite are detected only in the grey rock facies, and the crusts are observed only on the grey facies. Another reason is the observed pyrite oxidation and intermediate formation of a surface layer of recrystallized calcite, serving as reaction substrate for gypsum nucleation and growth (Fig. 7). It is also worth noting that gypsum precipitation occurs even for very low concentrations of CaO and pyrite [53]: in Taya

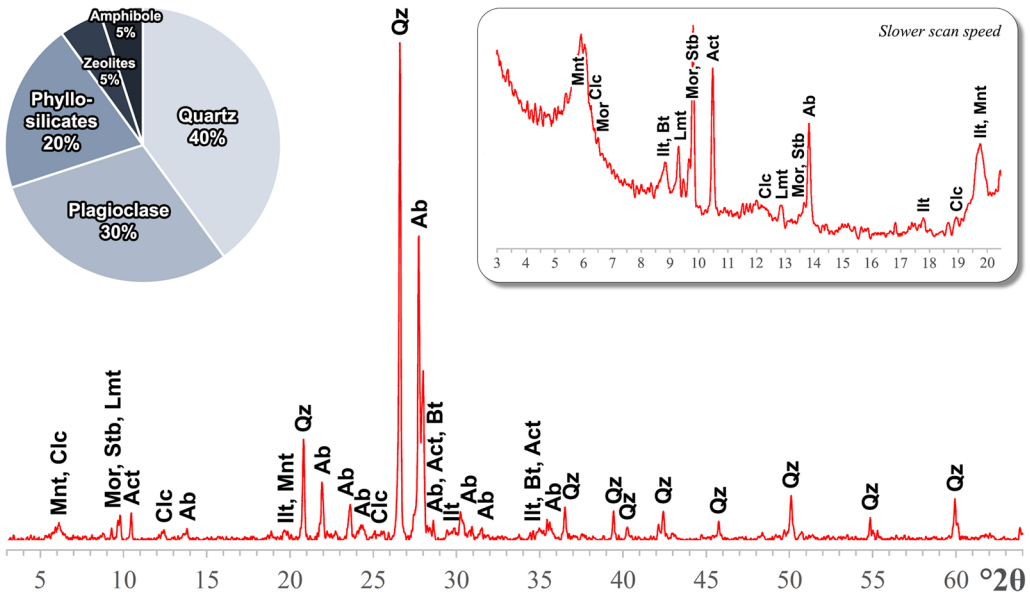

Fig. 5 Representative XRD pattern determined on Taya stone, with the average semi-quantitative composition of the major phases calculated via software (*Ab* albite, *Act* actinolite, *Bt* biotite, *Clc* clinochlore, *Ilt* illite, *Lmt* laumontite, *Mnt* montmorillonite, *Mor* mordenite, *Qz* quartz, *Stb* stilbite)

stone, CaO content is about 4%,[3] while SO_3 is 1.15% in the grey rock facies—clearly higher than in the brown facies (Table 2). A final clue is the chemical composition of the groundwater, in particular its enrichment in Ca^{2+} and SO_4^{2-} (Table 1). The rock-water chemical interaction occurs during the in-pore filtration of the slightly acid water from the rain or the surface streams, during which its pH slightly rises,[4] and after the capillary rise from the subsoil and lacustrine waters.

Figure 9 shows the reconstruction of one of the possible sequences of gypsum formation in Taya Caves. The process starts in the grey rock facies, rich in calcareous fossils and framboidal pyrite, mostly filling the shell internal pores. The pyrite inside intact bioclasts is virtually sealed, and limitedly interacts with the external microenvironment. When the bioclast walls are dissolved, pyrite becomes more reactive and can dissolve too, migrating, recrystallizing, and breaking down the former multi-framboids. The released pyrite can undergo oxidation, as suggested by microcrystal zonings (S-depletion of oxidized rims) and framboid substitutions (with pseudomorphs of Fe-oxides and hydroxides).

In conclusion, other possible mineral sources fueling gypsum precipitation need to be briefly mentioned, e.g., zeolites, plagioclase, and actinolite. However, their weathering is deemed more limited, as also suggested by the groundwater composition, namely by Na and Mg concentrations.

Other soluble salts

As for the other secondary phases detected in Taya Caves, particularly the salts in the efflorescences, possible external sources need to be taken into account, rather than the contribution of rock-forming minerals. In fact, the fresh Taya stone has Cl and P concentrations matching the typical low values of mudrocks [58], and does not contain halite, which represents the dominant chloride in marine sedimentary rocks [59]. In addition, Taya Caves do not contain deposits of bat guano or bones, representing possible sources of phosphates [60].

Then, the salt source is possibly the cropland for vegetable farming on Taya hill, above the cave vault, and the mineral agrochemicals used therein. No precise indications could be obtained from the landowners and no comparative soil analyses were carried out, which would both validate that assumption. However, the compositional correspondence between the efflorescences and some of the most traditional mineral-based chemicals used in agriculture is striking [61–65]. For instance, K-salts are extensively utilized as fertilizers, especially

[3] The CaO content in the brown and grey rock facies is similar, although the latter contains calcareous bioclasts. This is explained by the highly variable distribution, relative concentration, and grain size of the fossils. The same reason lies in the absent or weak signals of any carbonate mineral in the XRD patterns.

[4] Although the basic and acid products of $CaCO_3$ and pyrite dissolution may neutralize each other [55, 56], in this case the pH increase is supposed to depend on the somewhat greater contribution of the weathering of carbonates and other minerals releasing alkali ions [14].

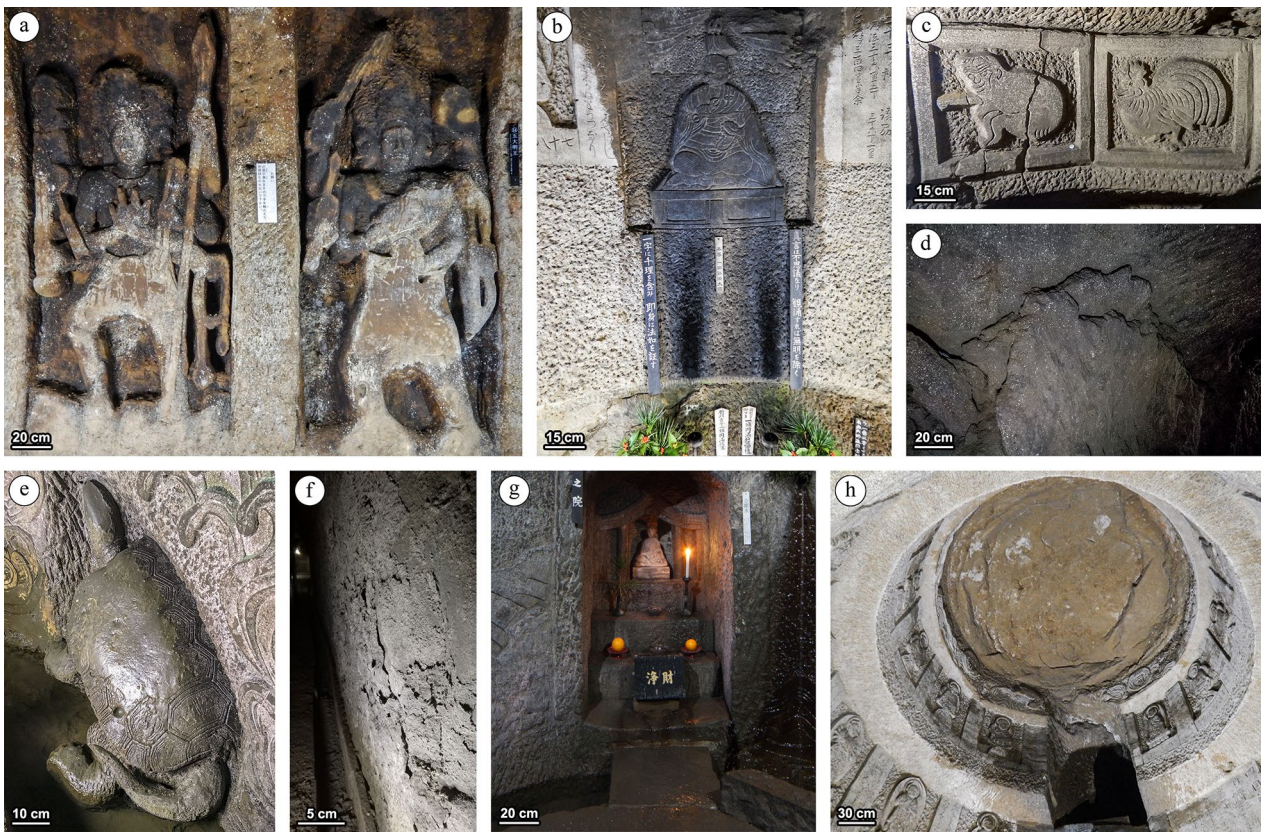

Fig. 6 Some of the stone deterioration patterns recognized in Taya Caves: erosion and rounding of the carved elements (**a**, **e**), black soiling and patinas (**a**, **b**), fractures (**c**), splitting (**d**), and peeling (**f**). The presence of flowing water is displayed in (**g**). The partial collapse of a sculpted ceiling is showed in (**h**)

sylvite (KCl), and also K-Mg chlorides and sulfates. Phosphates find a large application as fertilizers and pesticides too, mainly deriving from organic products, phosphate rocks and apatite, and commercialized as $Ca(H_2PO_4)_2{\cdot}H_2O$, at times mixed with gypsum. Chlorides and phosphates would represent the major agriculture-derived contribution to the efflorescences in Taya Caves. Pure gypsum and calcareous rocks are also widely used as fertilizers, pesticides, and soil amenders; in this case, however, the fossil and pyrite dissolution are the main source of the reprecipitated calcite and gypsum in the efflorescences.

Another concurrent factor is related to the soil of Taya hill, in particular to its extensive vegetation cover. The subsurface waters of forest soils are generally richer in the products of transpiration and decomposition of organic acids including, e.g., P, Cl, K, S, Ca, etc. [31, 34].

Similarly to the crusts, the efflorescences form after the percolation of water from rain or surface streams through the rock pores, carrying in solution the chemicals linked to the agrochemical use and vegetation cover, or water capillary rise. The groundwater composition also confirms the major chloride input and the acidity reduction (Table 1).

Environmental constraints

In Taya Caves, well-formed and coarse-grained crusts occur only in the entrance gallery and the Turtle hall. The efflorescences also occur in the entrance gallery, covering large surfaces on the lower walls, but are observable in the adjoining parallel exit gallery too. Only minor traces of chemical alteration are detected in the surrounding areas. That is the case, for instance, of the early-sulfation buffer zone, slightly deeper into the caves, namely in the Wisdom Kings hall, the Zodiac hall, and the inner sectors of the entrance gallery (cf. Figure 2).

It is clear that the crusts and efflorescences occur in the same or nearby cave zones. Their formation and stability are strongly influenced by microenvironmental factors, the most significant being air humidity and rock moisture, their fluctuations, and evaporation kinetics. These factors control salt crystallization, growth, degree of crystallinity, and cycles of crystallization/dissolution.

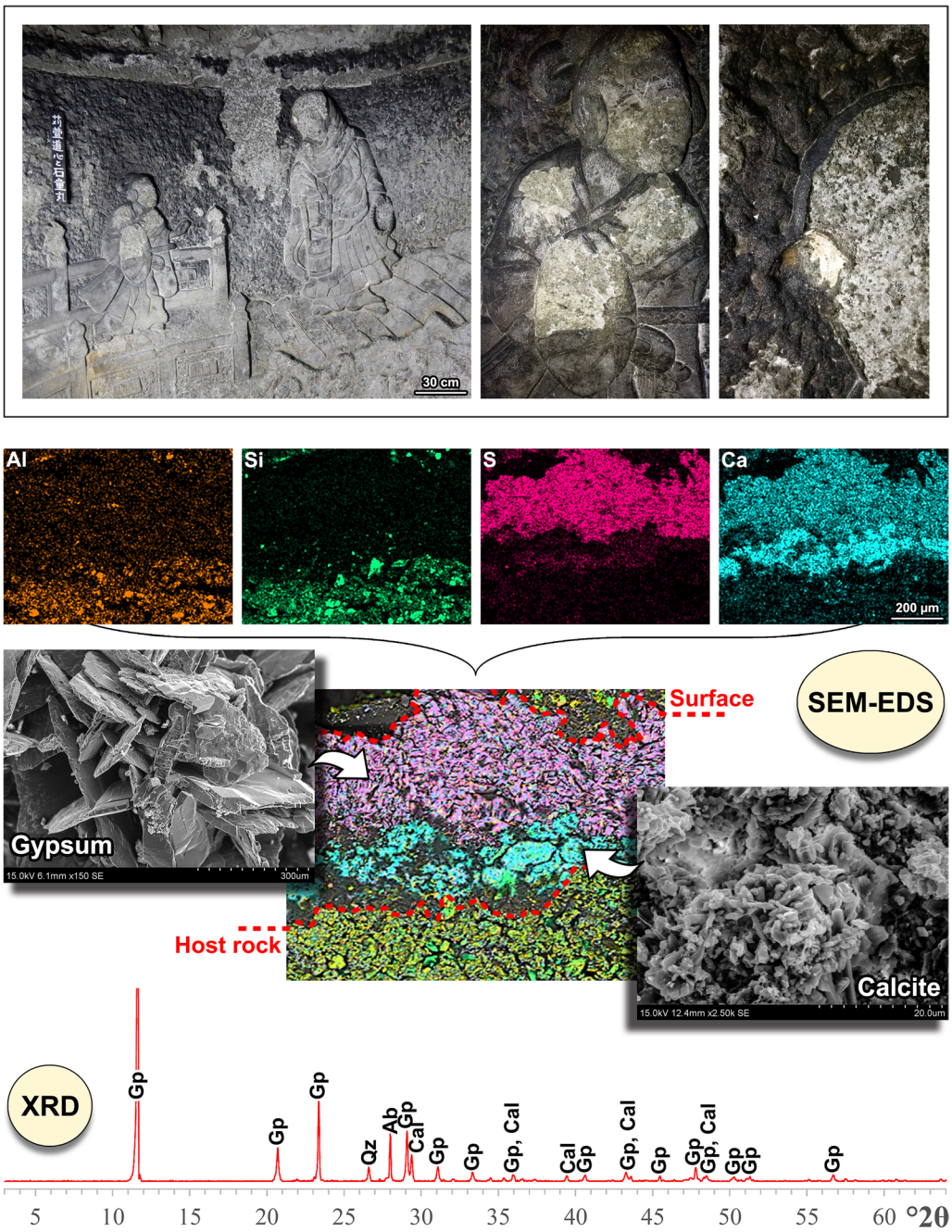

Fig. 7 Gypsum crusts deteriorating the carvings in the Turtle hall. Their chemical and mineralogical composition and stratigraphy are showed by the SEM–EDS observations and X-ray mappings, and the representative XRD pattern (*Ab* albite, *Cal* calcite, *Gp* gypsum, *Qz* quartz)

Generally, the driest areas of Taya Caves appear as the most intensely disturbed by salt weathering.

The secondary phases have diverse solubility and hygroscopicity. Gypsum, after calcite, has the lowest solubility and an extremely high deliquescence RH, higher than 99% [66], so it is potentially stable in many conditions, even very humid. However, gypsum does not precipitate or dissolves where RH remains at nearly constant 100%, e.g., in the innermost cave areas, and where the substrate is constantly wet (because of stronger vapor condensation or water runoff and dripping). On the contrary, unwet surfaces, lower mean RH [67], and more

Table 2 Bulk chemical composition of Taya stone, differentiating between the brown- and grey-colored facies, and samples representative of some weathering patterns, determined by XRF

	Rock		Weathering			
	Brown facies	Grey facies	Gypsum crusts	Early sulfation	Efflorescences	Orange patinas
Na_2O	1.74	1.74	0.20	1.74	1.60	1.02
MgO	2.37	3.58	0.53	3.26	2.90	1.85
Al_2O_3	16.67	16.19	1.73	15.39	14.82	9.25
SiO_2	60.07	57.66	5.78	55.38	54.68	40.53
P_2O_5	0.07	0.10	0.02	0.08	0.33	1.19
SO_3	0.03	1.15	38.79	2.32	1.07	0.15
K_2O	1.58	1.48	0.19	1.55	1.66	0.95
CaO	3.73	3.94	32.66	4.36	4.28	2.95
TiO_2	0.61	0.61	0.12	0.60	0.60	0.44
MnO	0.10	0.20	0.01	0.11	0.14	0.91
Fe_2O_3	6.37	6.76	0.97	6.69	6.86	26.33
LOI	6.47	6.43	18.92	8.34	10.75	14.24
Cl	159	219	186	156	1675	151
V	72	138	*bdl*	*bdl*	*bdl*	162
Cr	83	66	*bdl*	*bdl*	57	*bdl*
Ni	37	*bdl*	56	41	*bdl*	116
Cu	61	73	*bdl*	88	101	90
Zn	103	108	*bdl*	117	132	197
Br	*bdl*	*bdl*	31	21	213	*bdl*
Rb	62	57	*bdl*	57	54	52
Sr	367	429	381	434	331	343
Y	22	15	*bdl*	18	20	179
Zr	117	137	*bdl*	155	144	118
Ba	277	180	*bdl*	159	207	*bdl*

Major-element oxides and LOI are in wt%, trace elements in ppm

bdl stands for "below detection limit"

frequent and longer RH deviations from saturation, allow gypsum to crystallize and stabilize, for instance near the current and ancient gates (Fig. 3). Further closer to the cave entrance, where RH is the lowest, the efflorescences form: they contain salts with a significantly lower deliquescence RH compared to pure gypsum, and require a dryer environment [14, 68].

Nevertheless, reasoning in terms of salt mixtures, rather than pure phases, represents the best approach. In fact, the actual deliquescence RH of gypsum in Taya Caves is possibly lower, since the other salts in solution may considerably increase gypsum solubility [69, 70]. That applies especially to the surfaces with the efflorescences, where the concentration of the other salts is supposedly higher and solution supersaturation is easily reached after water evaporation: the chlorides play a leading role in increasing gypsum solubility [66], so that actual crusts and coarse-grained gypsum crystals cannot grow. This is also in agreement with previous studies reporting the formation of powdery gypsum patinas in less humid environments as opposed to gypsum crusts [70].

Rock-water physical interaction

Porosity

Taya stone is characterized by a very low density and extremely high porosity, being 42% on average and ranging from 40 to 47%, as determined by MIP. The pore-size distribution indicates that micropores (smaller than 0.1 μm) are in minority, i.e., on average 12% versus the 88% of the larger capillary pores. The unimodal distribution has a peak on pore size values slightly smaller than 10 μm (Fig. 10). No significant differences were found between the brown and the grey facies.

These data are very important for understanding the physical mechanisms of rock-water interaction. In fact, open porosity can control the intensity of water-related

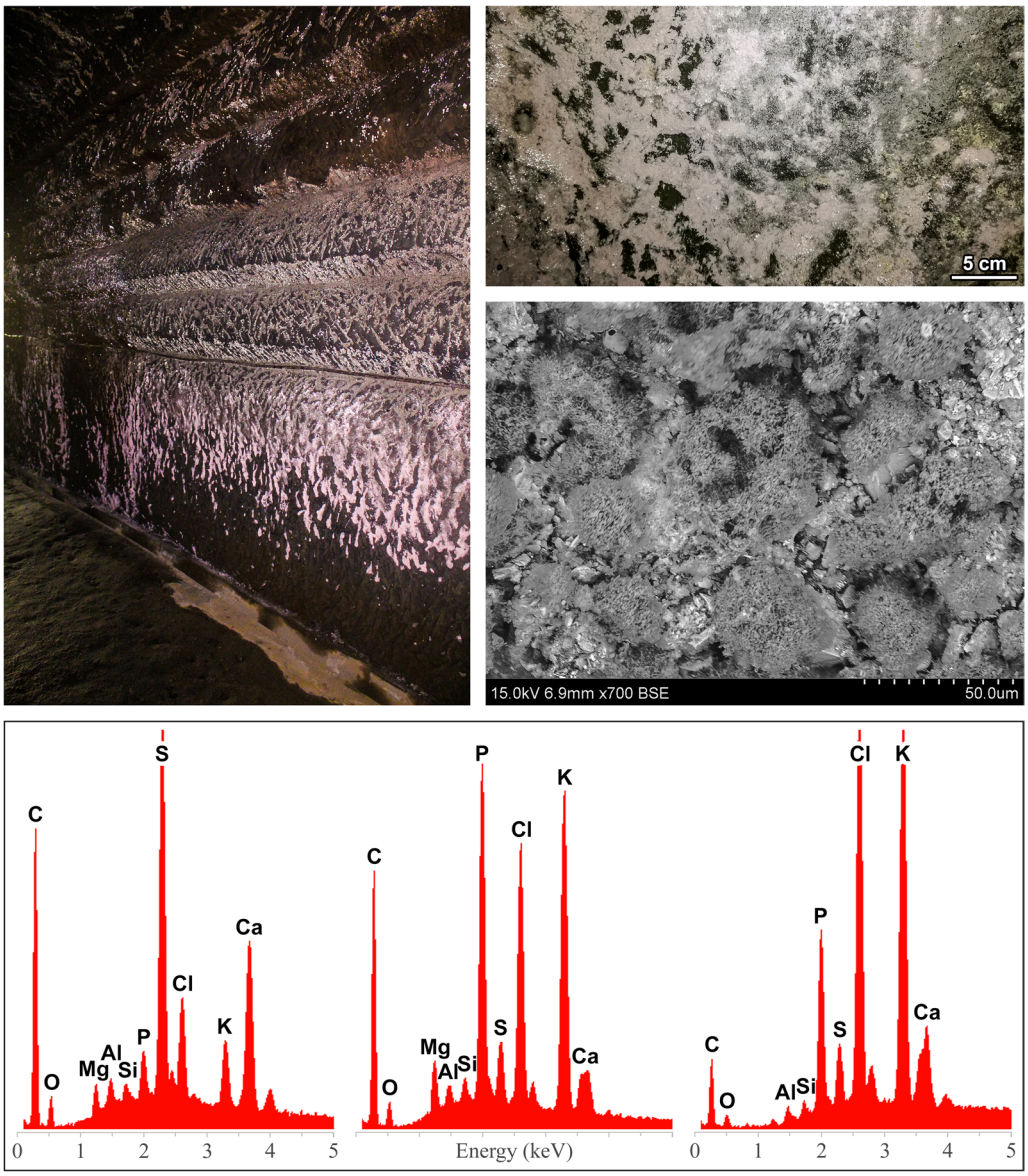

Fig. 8 Different observation scales of the efflorescences in Taya Caves (gallery, wall detail, and microscopic detail at the SEM-BSE), with their chemical composition summarized by the SEM–EDS microanalysis of three representative spots

weathering, and each pore-size class is preferentially involved in different processes.

Water absorption

Pore volume rules the amount of liquid water absorbed by the rock, but the process rate is markedly controlled by pore-size distribution [71, 72]. The mass increase of Taya stone in conditions of total immersion is prominent, about 25%, and extremely rapid, virtually running out after few tens of seconds (Fig. 11). Almost the totality of water is absorbed during the very first minute, because of the extremely high porosity, good pore interconnection, and almost exclusive presence of capillary pores that, together with macropores, are filled most quickly [73]. The minor influence of micropores, which are typically filled after longer times, cannot be easily assessed. In fact, at laboratory scale, the material is too weak and cannot withstand hour- or day-long immersions. The

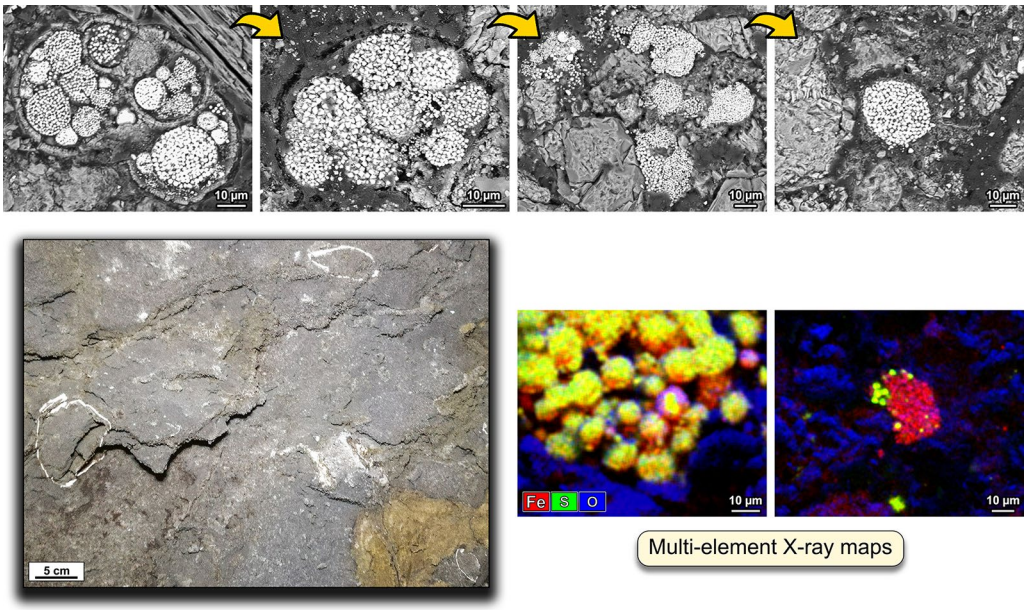

Fig. 9 SEM-BSE photomicrographs showing different spatial arrangements of pyrite (the white grains) in the grey facies of Taya stone, and EDS chemical maps with examples of pyrite oxidation and S depletion. The inset shows some coarse-grained calcareous fossils on the walls of Taya Caves

testing turned out to be very troublesome—due to early cracking and disintegration—even for large specimens (up to 1 kg). It is worth noting, however, that variations of water content can cause major changes in the mechanical performance of the stone [74], but the actual resistance of the rock mass in the caves is higher.

Hygroscopic water adsorption

Pore size has also a dramatic impact on hygroscopic water adsorption. The maximum condensation-related mass increase of Taya stone is 4% on average (at 98% RH), obviously much lower compared to liquid water absorption. It is worth noting the adsorption trend. Up to 90% RH, the mass increase is nearly linear, corresponding to 0.1–0.3% for every increase of 5% of RH, then the trend clearly becomes steeper: at the final stage, with extremely high humidity, the mass increase reaches about 1%, corresponding to 1/4 of the total hygroscopic water that the stone can adsorb. The desorption curves follow the relevant adsorption trends, pointing out a rapid loss of water down to 85%. A certain degree of hysteresis is noticeable, indicating the permanence of residual water stored in the pores (Fig. 11). Summarizing, RH fluctuations are particularly critical around 90%, since they can cause the strongest variations of adsorbed or desorbed water vapor and related mass changes, especially approaching air saturation. Hygroscopic adsorption is often more significant for micropores: in fact, water vapor can condensate inside pores even when RH is lower than 100%, but the smaller the pore the lower the adsorption RH [75]. However, the prevailing larger capillary pores in Taya stone require an extremely high RH for hygroscopic adsorption to take place, equal to 95% or higher. As for the differences between the brown and grey facies, their behavior is practically identical, with the exception that the brown rock type shows a slightly higher adsorption.

Slake durability

The definition of slaking is slightly changing in the literature, but generally indicates a form of rock disintegration resulted from the direct interaction with water in liquid and/or vapor state (e.g., partial contact or immersion, alternate wetting/drying, exposure to air humidity) [76, 77]. Taya stone turned out to have a surprisingly low slake durability. At laboratory scale, most specimens begin crumbling right after the water immersion, with some differences between the brown and grey rock type during the early stage: the grey type may not show massive disintegration in the first 10–15 min, whereas the brown type may face advanced decay, with extensive cracking and crumbling already in the very first minutes, until the specimen turns quickly into a heap of chips and flakes or a mud-like mass. These last conditions are reached in few hours by the grey rock type too (Fig. 11). The diverse

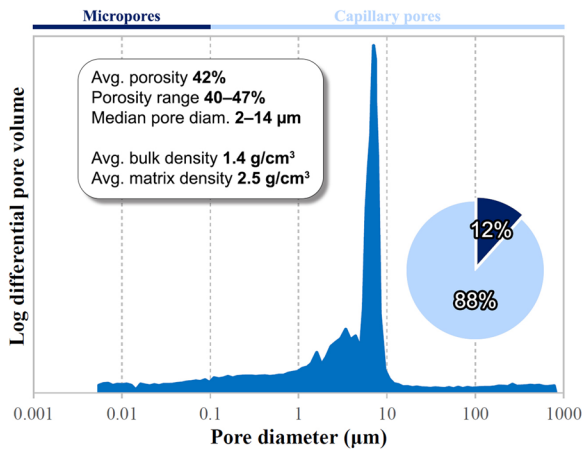

Fig. 10 Representative MIP data of porosity, pore-size distribution, and other related properties, determined on Taya stone

timings might be explained by the only major textural difference between the two facies, namely the presence of harder fossil shells, acting somewhat as a structural reinforcing component of the rock matrix.

Slake deterioration related to water absorption is mainly caused by: (1) the mechanical action of water on the weak intercrystalline bonds; (2) swelling-induced stresses, especially the volume changes of expansive clay minerals, in particular smectites (montmorillonite volume increases two-fold [78]); (3) the tensile stresses generated by the air entrapped in voids and discontinuities and pressurized as water is absorbed. The weathering is particularly severe for Taya stone due to the high and fast water absorption and the abundance of clay minerals. The related deformations and mechanical stresses may be exacerbated when water absorption alternates cyclically with drying processes, during which clay minerals dehydrate and shrink and negative suction pressures develop in the pores. This also happens with cycling hygroscopic adsorption/desorption [26, 53, 76, 79], which recurs more frequently near the cave entrance, just in the mentioned RH critical range (90–100%).

Conservation issues

The preservation of a semi-natural site like Taya Caves and of the rock art enshrined therein is difficult to put in practice, considering that the first measure to adopt would be to keep the microenvironmental parameters as constant as possible. Dealing with stone preservation means dealing with the safeguard of the whole site. Here, the general key points to address in a future conservation campaign will be highlighted.

Overall, stone weathering in Taya Caves is principally due to a combination of the following major factors:

- Water absorption/adsorption and related cycles;
- Mineral dissolution, mobilization, and precipitation and related cycles;
- Land use and vegetation cover of Taya hill;
- Structural instability due to static problems and earthquakes.

Rock-water chemical and physical interaction poses probably the highest risk. Although that is a constant process in Taya Caves, it might upsurge due to exceptional events associated with major increases of water flow rate, e.g., in summer and early fall, when most precipitations are concentrated and typhoons occur. Wetting/drying cycles need also to be taken into consideration, both temporally—i.e., the alternation of rainy and fair days, more frequent in the rainy season—and spatially—that is, more cycles occur in the cave areas affected by external airflows.

Different degrees of weathering susceptibility can be traced in different cave sectors. Taya Caves are a relatively homogeneous semi-closed system, but the near-entrance and near-surface areas represent an exception and demand attention. There, the lower and more variable humidity and moisture trigger salt weathering. Soluble salts react differently to environmental changes if compared to the rock, concerning the cyclic processes of crystallization/dissolution, hydration/dehydration, hygroscopic adsorption/desorption, etc. These processes cause mechanical fatigue, strongly localized at the interface with the rock, which eventually leads to major disintegrations.

Finally, with regard to the conservation or restoration interventions done so far, the most important involved the arrangements for setting up the show cave, occasional safety measures and targeted works of wall reinforcement and reconstruction, and the installation of a door at the entrance. Moreover, it is worth reporting the recent digital reconstructions in three-dimensional models of the topography and morphology of Taya Caves [80, 81]; this represents the first step to pass on their history and beauty to the next generations, and may support the future evaluation of deterioration rate.

Summary and conclusions

The history and rock art enshrined in Taya Caves, their allure, and the urge to comprehend, preserve, and promote their cultural value led to this first-ever scientific investigation, dealing with the stone properties, deterioration, and environmental setting.

Taya Caves are a composite system of underground halls and galleries excavated and carved into a Pleistocene clay-rich fossiliferous siltstone. The rock is extremely soft and porous, yet the caves and their

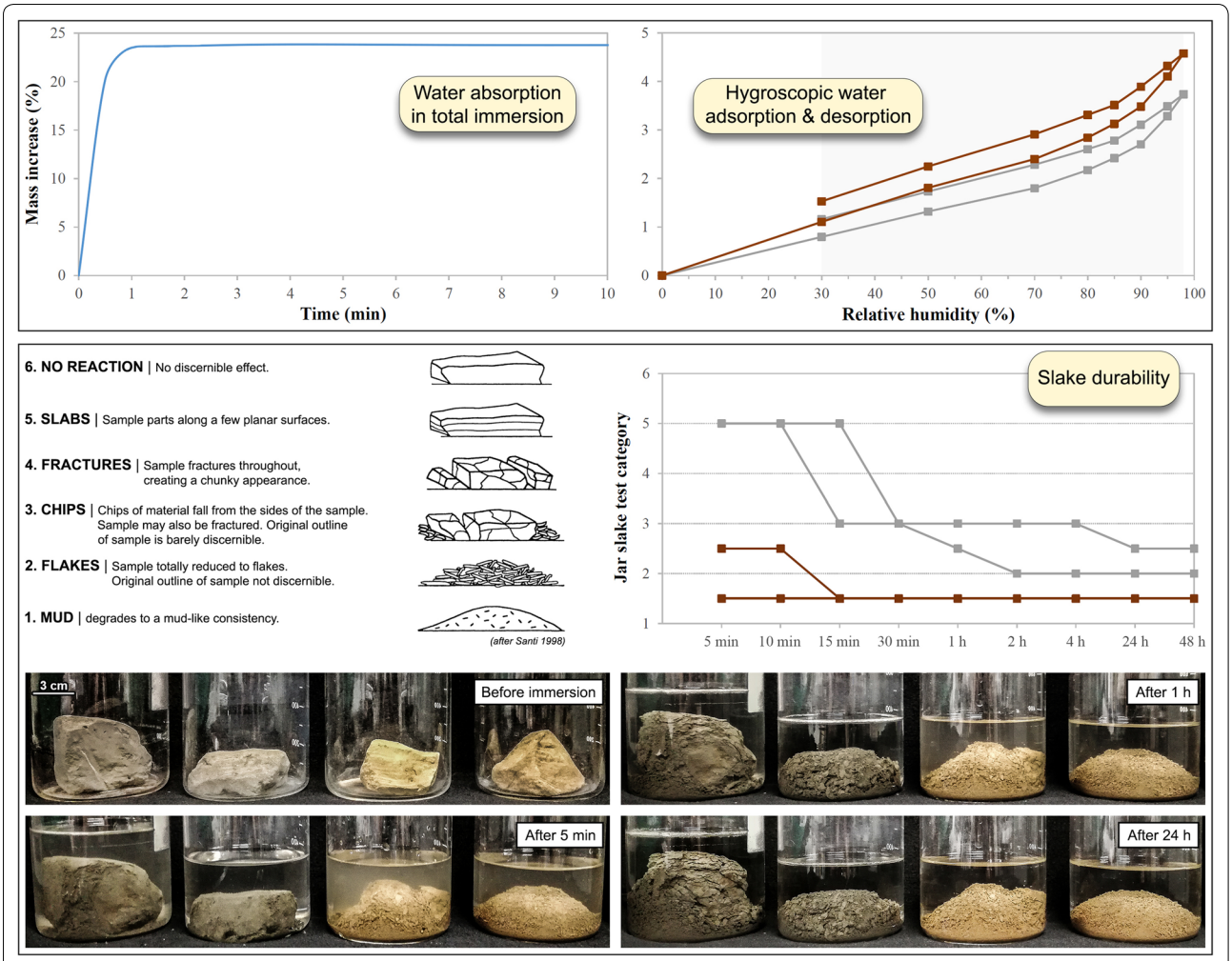

Fig. 11 Physical interaction of Taya stone with water: representative trends of mass change by water absorption in total immersion at atmospheric pressure and by hygroscopic water adsorption/desorption in the shaded RH range (*upper box*); slake durability, determined in total immersion in water by the jar slake test (*lower box*). When differentiating between the brown and grey rock facies, the 2 different colors are used in the graphs

sculptural heritage still survive. The ongoing stone deterioration, however, poses a threat to the site preservation, as indicated by cracking, detachments, material losses, surface alteration, and biological colonization. The highest risk is placed by water and its chemical and mechanical action on the stone. Water represents a constant in Taya Caves, either flowing, dripping, and stagnant; or rising from the subsoil; or related to the extremely high RH, close to 100%.

During infiltration and percolation of rainwater and surface water, capillary rise, or vapor condensation, cyclic processes of mineral dissolution, mobilization, and precipitation occur. Their marker is the formation of crusts and efflorescences on the cave walls. The crusts are mainly constituted by gypsum, crystallized from the reaction of the dissolution products of calcareous bioclasts and pyrite minerals; calcite is also detected as minor component. The efflorescences, instead, are composed of mixed chlorides, phosphates, sulfates, and carbonates: considering the presence of a cropland above the cave vault, they might possibly derive from agrochemicals (especially sylvite- and apatite-based), or from the surface vegetation cover. The groundwater composition, enriched in Ca^{2+}, SO_4^{2-}, and Cl^-, provides further confirmations. Crusts and efflorescences only occur in the driest cave areas, the closest to the entrance or surface, in the southern side—apart from those, the cave microclimate is characterized by highly stable temperature and RH. The modes and mechanisms of salt weathering and cycles of salt dissolution/recrystallization are related to

the following parameters: phase solubility, hygroscopicity, and deliquescence; microenvironmental variables, i.e., RH, rock moisture, and evaporation kinetics; in-pore water mineralization and supersaturation. The most stable secondary phase turns out to be gypsum; its crystallization, however, may occur only on unwet substrates and where the air is not constantly water-saturated.

Rock-water interaction is particularly damaging even considering just the physical mechanisms. The siltstone of Taya Caves features a very high and fast absorption of liquid water, and a more contained yet significant adsorption of hygroscopic water, especially when the RH is higher than 90%—these processes are ruled by the high porosity and the specific pore-size distribution controlled by capillary pores. The slake durability is extremely low: as water is absorbed, the mechanical stresses generated by in-pore water and air movement and the swelling clay minerals may lead to rapid disintegration phenomena. These are exacerbated by cycles of wetting/drying and hygroscopic adsorption/desorption, occurring more often where the microclimate is changing and affected by external airflows. In other terms, the cave areas near the entrance or surface present again an increased decay susceptibility.

The scientific questions about Taya Caves have not been all answered, and further work needs yet to be done. Interesting insights might be provided, for instance, by targeted investigations of the structural stability, the engineering properties of the rock mass, and the related risk to visitor safety; or the actual damage brought about by the microbiological colonization.

Concluding, there is no doubt that the intrinsic vulnerability of Taya Caves requires constant monitoring, complemented by extraordinary surveys, particularly after extreme natural events (intense precipitations and typhoons, earthquakes) or changes of the visitor flow. The information provided in this study can aid those activities. Furthermore, this first research is expected to raise concerns about the cave safeguard and support future, more organic conservation plans. Finally, it will hopefully foster a wider promotion and valorization of this heritage site.

Supplementary information

Supplementary information accompanies this paper at https://doi.org/10.1186/s40494-020-00433-9.

Additional file 1. Map of Taya Caves, with the location of the monitoring and sampling spots.

Abbreviations

RH: Relative humidity; IC: Ion chromatography; SEM: Scanning electron microscope (SEM); SE: Secondary electrons; BSE: Back-scattered electrons; EDS: Energy-dispersive X-ray spectroscopy; XRD: X-ray diffraction; XRF: X-ray fluorescence; WDS: Wavelength-dispersive X-ray spectroscopy; LOI: Loss on ignition; MIP: Mercury intrusion porosimetry.

Acknowledgements

The authors thank the following people for supporting the experimental work: S. Hossain, T. Kuroda, K. Okamoto, M. Osada, T. Saito, K. Sakane, M. Tokunaga. The photos of the interior of Taya Caves are by the authors, the Executive Committee for the Preservation of Taya Cavern, and S. Sonoda. The map is by the Executive Committee with edits by the authors.

Authors' contributions

LG: conceptualization, methodology, validation, formal analysis, investigation, writing—original draft, writing—review & editing, visualization, funding acquisition. CTO: conceptualization, methodology, investigation, resources, writing—review & editing, supervision, project administration, funding acquisition. YT: investigation, resources. SA: investigation. MO: investigation. All authors read and approved the final manuscript.

Funding

This work was supported by JSPS (Japan Society for the Promotion of Science), under an international postdoctoral fellowship granted to L. Germinario (ID no. P18122—Standard).

Availability of data and materials

The datasets used and/or analysed during the current study are available from the corresponding author on reasonable request.

Competing interests

The authors declare that they have no competing interests.

Author details

[1] Department of Civil and Environmental Engineering, Saitama University, 255 Shimo-Okubo, Sakura-ku, Saitama-shi, Saitama-ken 338-8570, Japan. [2] Executive Committee for the Preservation of Taya Cavern, 271-1-201 Yabe-cho, Totsuka-ku, Yokohama-shi, Kanagawa-ken 244-0002, Japan.

Received: 25 May 2020 Accepted: 17 August 2020
Published online: 01 September 2020

References

1. Bonsall C, Tolan-Smith C, editors. The human use of caves. BAR International Series, 667. Oxford: Archaeopress; 1997.
2. Moyes H, editor. Sacred darkness: a global perspective on the ritual use of caves. Boulder: University Press of Colorado; 2013.
3. Ontañon R, Bayarri V, Herrera J, Gutierrez R. The conservation of prehistoric caves in Cantabria, Spain. In: Saiz-Jimenez C, editor. The conservation of subterranean cultural heritage. London: CRC Press; 2014. p. 185–192.
4. Malaurent P, Brunet J, Lacanette D, Caltagirone JP. Contribution of numerical modelling of environmental parameters to the conservation of prehistoric cave paintings: the example of Lascaux Cave. Conserv Manage Archaeol Sites. 2006;8(2):59–76.
5. Álvarez I, Bodego A, Aranburu A, Arriolabengoa M, del Val M, Iriarte E, Abendaño V, Calvo JI, Garate MD, Hermoso de Mendoza A, Ibarra F, Legarrea J, Tapia SJ, Agirre MJ. Geological risk assessment for rock art protection in karstic caves (Alkerdi Caves, Navarre, Spain). J Cult Herit. 2018;33:170–80.
6. Deacon J. Rock art conservation and tourism. J Archaeol Method Theory. 2006;13(4):379–99.

7. Saiz-Jimenez C. Cave conservation: a microbiologist's perspective. In: Cheeptham N, editor. Cave microbiomes: a novel resource for drug discovery. New York: Springer; 2013. p. 69–84.
8. Hoyos M, Soler V, Cañaveras JC, Sánchez-Moral S, Sanz-Rubio E. Microclimatic characterization of a karstic cave: human impact on microenvironmental parameters of a prehistoric rock art cave (Candamo Cave, northern Spain). Environ Geol. 1998;33:231–42.
9. Sánchez-Moral S, Soler V, Cañaveras JC, Sanz-Rubio E, Van Grieken R, Gysels K. Inorganic deterioration affecting the Altamira Cave, N Spain: quantitative approach to wall-corrosion (solutional etching) processes induced by visitors. Sci Total Environ. 1999;243(244):67–84.
10. Brunet J, Vouvé J, Malaurent P. Re-establishing an underground climate appropriate for the conservation of the prehistoric paintings and engravings at Lascaux. Conserv Manage Archaeol Sites. 2000;4:33–45.
11. Bourges F, Genthon P, Genty D, Lorblanchet M, Mauduit E, D'Hulst D. Conservation of prehistoric caves and stability of their inner climate: Lessons from Chauvet and other French caves. Sci Total Environ. 2014;493:79–91.
12. Vieten R, Winter A, Samson AVM, Cooper J, Wrapson L, Kambesis P, Lace MJ, Nieves MA. Quantifying the impact of human visitation in two cave chambers on Mona Island (Puerto Rico): implications for archaeological site conservation. Cave Karst Sci. 2016;43(2):79–85.
13. ICOMOS. Illustrated glossary on stone deterioration patterns. Paris: ICOMOS, Monuments and Sites, XV; 2010.
14. Steiger M, Charola AE, Sterflinger K. Weathering and deterioration. In: Siegesmund S, Snethlage R, editors. Stone in architecture. Properties, durability. 5th ed. Berlin: Springer; 2014. p. 225–316.
15. Gázquez F, Rull F, Medina J, Sanz-Arranz A, Sanz C. Linking groundwater pollution to the decay of 15th-century sculptures in Burgos Cathedral (northern Spain). Environ Sci Pollut Res. 2015;22:15677–89.
16. Williams P. World Heritage caves and karst. Gland: IUCN; 2008.
17. Saiz-Jimenez C, editor. The conservation of subterranean cultural heritage. London: CRC Press; 2014.
18. Hildreth-Werker V, Werker JC. Cave conservation and restoration. Huntsville: National Speleological Society Inc.; 2006.
19. Doehne E, Price CA. Stone conservation. An overview of current research. 2nd ed. Los Angeles: The Getty Conservation Institute; 2010.
20. Le Huu P. Buddhist architecture. Lakeville: Grafikol s.l.; 2010.
21. Sharf R. Art in the dark: the ritual context of Buddhist caves in western China. In: Park D, Wangmo K, Cather S, editors. Art of merit: studies in Buddhist art and its conservation. London: Archetype Publications; 2013. p. 38–65.
22. Ogata K. (2019) The artistic qualities of religion reliefs in Taya-cave, Japan. In: JpGU Meeting 2019, 26–30 May 2019, Chiba, Japan
23. ASTM D4404-84. Standard test method for determination of pore volume and pore volume distribution of soil and rock by mercury intrusion porosimetry. West Conshohocken: ASTM; 1998.
24. EN 13755. Natural stone test methods—determination of water absorption at atmospheric pressure. Brussels: CEN; 2008.
25. EN ISO 12571. Hygrothermal performance of building materials and products - Determination of hygroscopic sorption properties. Brussels: CEN; 2000.
26. Santi PM. Improving the jar slake, slake index, and slake durability tests for shales. Environ Eng Geosci. 1998;4(3):385–96.
27. JMA. Japan Meteorological Agency—General Information on climate of Japan. 2020. https://www.data.jma.go.jp/gmd/cpd/longfcst/en/tourist.html. Accessed 22 Jan 2020
28. JMA. Japan Meteorological Agency – Past weather data of Yokohama. 2020. https://www.data.jma.go.jp/obd/stats/etrn/index.php?prec_no=46&block_no=47670&year=&month=&day=&view. Accessed 22 Jan 2020
29. JMA. Japan Meteorological Agency – Typhoon statistics. 2020. https://www.data.jma.go.jp/fcd/yoho/typhoon/statistics. Accessed 22 Jan 2020
30. Livingstone DA. Chemical composition of rivers and lakes—Chapter G. In: Fleischer M, editor. Data of geochemistry. 6th ed. Washington: Geological Survey Professional Paper 440-G United States Government Printing Office; 1963. p. 1–64.
31. Kocharyan AG. Ground and soil water characteristics. In: Khublaryan MG, editor. Types and properties of water, vol. 2. Oxford: EOLSS/UNESCO; 2009. p. 117–135.
32. Nikanorov AM, Brazhnikova LV. Water chemical composition of rivers, lakes and wetlands. In: Khublaryan MG, editor. Types and properties of water, vol. 2. Oxford: EOLSS/UNESCO; 2009. p. 42–78.
33. Bhateria R, Jain D. Water quality assessment of lake water: a review. Sustain Water Res Manag. 2016;2:161–73.
34. Shestopalov VM. Typification of groundwater characteristics. In: Khublaryan MG, editor. Types and properties of water, vol. 1. Oxford: EOLSS/UNESCO; 2009. p. 95–118.
35. Nakagawa H. Structural growth of the Kanto Tectonic Basin. Science Reports of Tohoku University, 2nd series (Geology). 1962;5:373–393.
36. Mitsunashi T, Kikuchi T. Geology of the Yokohama district. Tsukuba: Geological Survey of Japan; 1982.
37. Ozawa H. Middle Pleistocene ostracods from the Naganuma Formation, Sagami Group, central Japan: significance of the occurrence for the bay fauna along the Northwest Pacific margin. Paleontol Res. 2009;13(3):231–44.
38. Wilkin RT, Barnes HL. Formation processes of framboidal pyrite. Geochim Cosmochim Acta. 1997;61(2):323–39.
39. Merinero R, Lunar R, Martínez-Frías J, Somoza L, Díaz-del-Río V. Iron oxyhydroxide and sulphide mineralization in hydrocarbon seep-related carbonate submarine chimneys, Gulf of Cadiz (SW Iberian Peninsula). Mar Pet Geol. 2008;25:706–13.
40. Berner RA. Sedimentary pyrite formation: An update. Geochim Cosmochim Acta. 1984;48:605–15.
41. Fisher I, St J, Hudson J.D. Pyrite geochemistry and fossil preservation in shales. Philosophical Transactions of the Royal Society of London—Series B. 1962:311;167–169
42. Fisher I, St J. Pyrite replacement of mollusc shells from the Lower Oxford Clay (Jurassic) of England. Sedimentology. 1986;33:575–85.
43. Germinario L, Siegesmund S, Maritan L, Simon K, Mazzoli C. Trachyte weathering in the urban built environment related to air quality. Herit Sci. 2017;5:44. https://doi.org/10.1186/s40494-017-0156-z.
44. Farkas O, Siegesmund S, Licha T, Török Á. Geochemical and mineralogical composition of black weathering crusts on limestones from seven different European countries. Environ Earth Sci. 2018;77:211.
45. Germinario L, Török Á. Surface weathering of tuffs: compositional and microstructural changes in the building stones of the medieval castles of Hungary. Minerals. 2020;10(4):376. https://doi.org/10.3390/min10040376.
46. Choquette PW, Pray LC. Geologic nomenclature and classification of porosity in sedimentary carbonates. Am Assoc Pet Geol Bull. 1970;54(2):207–50.
47. Plummer LN, Wigley TML, Parkhurst DL. The kinetics of calcite dissolution in CO_2-water systems at 5° to 60°C and 0.0 to 1.0 atm CO_2. Am J Sci. 1978;278:179–21616.
48. Busenberg E, Plummer LN. A comparative study of the dissolution and crystal growth kinetics of calcite and aragonite. In: Mumpton FA, editor. Studies in diagenesis. Washington: Geological Survey Bulletin 1578. United States Government Printing Office; 1986. p. 139–168.
49. Arvidson RS, Evren EI, Amonette JE, Luttge A. Variation in calcite dissolution rates: a fundamental problem? Geochim Cosmochim Acta. 2003;67(9):1623–34.
50. Ruiz-Agudo E, Putnis CV, Rodriguez-Navarro C, Putnis A. Effect of pH on calcite growth at constant aCa^{2+}/aCO_3^{2-} ratio and supersaturation. Geochim Cosmochim Acta. 2011;75:284–96.
51. De Moel PJ, Van der Helm AWC, Van Rijn M, Van Dijk JC, Van der Meer WGJ. Assessment of calculation methods for calcium carbonate saturation in drinking water for DIN 38404–10 compliance. Drink Water Eng Sci. 2013;6:115–24.
52. Korchef A, Touaibi M. Effect of pH and temperature on calcium carbonate precipitation by CO_2 removal from iron-rich water. Water Environ J. 2019. https://doi.org/10.1111/wej.12467.
53. Taylor RK. Coal Measures mudrocks: composition, classification and weathering processes. Q J Eng Geol. 1988;21:85–99.
54. Larkin N. Pyrite decay: cause and effect, prevention and cure. NatSCA News. 2011;21:35–433.
55. Deer WA, Howie RA, Zussman J. An introduction to the rock-forming minerals. 3rd ed. London: The Mineralogical Society; 2013.
56. Ritsema CJ, Groenenberg JE. Pyrite oxidation, carbonate weathering, and gypsum formation in a drained potential acid sulfate soil. Soil Sci Soc Am J. 1993;57:968–76.

57. Weber PA, Stewart WA, Skinner WM, Weisener CG, Thomas JE, Smart R, St C. Geochemical effects of oxidation products and framboidal pyrite oxidation in acid mine drainage prediction techniques. Appl Geochem. 2004;19:1953–74.
58. Turekian KK, Wedepohl KH. Distribution of the elements in some major units of the Earth's crust. Geol Soc Am Bull. 1961;72:175–92.
59. Johns WD, Huang WH. Distribution of chlorine in terrestrial rocks. Geochim Cosmochim Acta. 1967;31:35–49.
60. Onac BP. Minerals in caves. In: White WB, Culver DC, Pipan T, editors. Encyclopedia of caves. 3rd ed. London: Elsevier; 2019. p. 699–709.
61. Wolfbauer CA. Mineral resources for agricultural uses. In: Lockeretz W, editor. Agriculture and Energy. New York: Elsevier; 1977. p. 301–314.
62. Manning DAC. Introduction to industrial minerals. London: Chapman & Hall; 1995.
63. Van Straaten P. Agrogeology: the use of rocks for crops. Cambridge: Enviroquest Ltd.; 2007.
64. Manning DAC. Phosphate minerals, environmental pollution and sustainable agriculture. Elements. 2008;4:105–8.
65. FAO. FAOSTAT—Food and Agriculture Organization of the United Nations. 2020. https://www.fao.org/faostat/en/#compare. Accessed: 7 May 2020
66. Charola AE, Pühringer J, Steiger M. Gypsum: a review of its role in the deterioration of building materials. Environ Geol. 2007;52:339–52.
67. Gázquez F, Calaforra JM, Evans NP, Hodell DA. Using stable isotopes ($\delta^{17}O$, $\delta^{18}O$ and δD) of gypsum hydration water to ascertain the role of water condensation in the formation of subaerial gypsum speleothems. Chem Geol. 2017;452:34–46.
68. Arnold A., Zehnder K. Salt weathering on monuments. In: Zezza F, editor, The conservation of monuments in the Mediterranean Basin—Proceedings of the 1st International Symposium, Bari, 7–10 Jun 1989. Grafo, s.l.; 1990. pp. 31–58
69. Price C, Brimblecombe P. Preventing salt damage in porous materials. Stud Conserv. 1994;39(sup2):90–3.
70. Zehnder K. Gypsum efflorescences in the zone of rising damp. Monitoring of slow decay processes caused by crystallizing salts on wall paintings. In: Riederer J, editor. Proceedings of the 8th International Congress on Deterioration and Conservation of Stone Berlin, 30 Sept–4 Oct 1996. Möller Druck: Berlin; 1996. pp. 1669–1678
71. Germinario L, Siegesmund S, Maritan L, Mazzoli C. Petrophysical and mechanical properties of Euganean trachyte and implications for dimension stone decay and durability performance. Environ Earth Sci. 2017;76:739. https://doi.org/10.1007/s12665-017-7034-6.
72. Germinario L, Török Á. Variability of technical properties and durability in volcanic tuffs from the same quarry region—examples from Northern Hungary. Eng Geol. 2019;262:105319. https://doi.org/10.1016/j.enggeo.2019.105319.
73. Siegesmund S, Dürrast H. Physical and mechanical properties of rocks. In: Siegesmund S, Snethlage R, editors. Stone in architecture. Properties, durability. 5th ed. Berlin: Springer; 2014. p. 97–224.
74. Oguchi C.T., Akimoto Y., Tamura Y., Sakane K. Physical and mechanical properties for damage assessment of Taya Cave rocks, central Japan. In: JpGU Meeting 2019, 26–30 May 2019, Chiba, Japan; 2019.
75. Camuffo D. Physical weathering of stones. Sci Total Environ. 1995;167:1–14.
76. Bell FG. Engineering geology. 2nd ed. Oxford: Elsevier; 2007.
77. Jeremias FT, Montero OJ, Pinho AB, Duarte IMR, Saroglou H, Torres Suárez MC. Mudrocks as soft rocks: properties and characteristics. In: Kanji M, He M, Ribeiro e Sousa L, editors. Soft rock mechanics and engineering. Cham: Springer; 2020. p. 37–108.
78. Madsen FT, Müller-Vonmoos M. The swelling behaviour of clays. Appl Clay Sci. 1989;4:143–56.
79. Czerewko MA, Cripps JC. Assessing the durability of mudrocks using the modified jar slake index test. Q J Eng Geol Hydrogeol. 2001;34:153–63.
80. Oguchi C.T, Shimizu K., Tamura Y., Hayakawa Y., Ogura T. (2020). An attempt of SfM photogrammetry to narrow and dark underground building heritage, EGU2020-9774. In: EGU General Assembly 2020, 3–8 May 2020, Vienna, Austria
81. Hayakawa Y.S., Ogura T., Tamura Y., Oguchi C.T. (2020). Representation of three-dimensional cave structure using point cloud data by terrestrial and airborne laser scanning. In: JpGU-AGU Joint Meeting 2020, 12–16 July 2020, Online

Publisher's Note